6-1-1987

High Rydberg states of an atom in parallel electric and magnetic fields

Robert Leonard Waterland

J. B. Delos

M. L. Du

High Rydberg states of an atom in parallel electric and magnetic fields

R. L. Waterland, J. B. Delos,* and M. L. Du*

Physics Department, College of William and Mary, Williamsburg, Virginia 23185

(Received 12 December 1986)

We have calculated the energy spectrum of a highly excited atom in parallel electric and magnetic fields. The eigenvalues were obtained by semiclassical quantization of action variables calculated from first-order classical perturbation theory. For the field strengths studied, the electron moves on a Kepler ellipse whose orbital parameters evolve slowly in time, and first-order perturbation theory reduces the problem to just one degree of freedom. Action variables were calculated from perturbation theory and the eigenvalues were obtained by semiclassical quantization of the action. The semiclassical analysis leads directly to a correlation diagram which connects the eigenstates of the Stark effect to those of the diamagnetic effect. A classification scheme for the eigenstates is proposed. Comparison with first-order degenerate quantum perturbation theory verifies the accuracy of the semiclassical treatment.

I. INTRODUCTION

In recent years there has been great interest in the effects of static fields on highly excited atoms.[1] Theoretical interest stems in part from the elegant experiments carried out in groups led by Kleppner, Liberman, Littman, and others.[2] Additional motivation arises from the fact that for such systems the Schrödinger equation and the Hamilton-Jacobi equation are very simple and well defined, but not separable. As a consequence, the classical trajectories show both regular and irregular motion, and the wave functions must under appropriate conditions manifest some form of "quantum chaos." Therefore, these seemingly simple problems reveal a surprising variety of behavior, and it is likely that much remains to be discovered.

Classical mechanics is particularly useful in the study of highly excited atoms for several reasons. First, quantum calculations on such systems are usually difficult. If the fields are weak, then, as we shall show in this paper, quantum perturbation theory easily leads to accurate results. More generally, however, a quantum calculation would involve an expansion in a very large basis.[3,4] Second, since excited atoms are close to the classical limit, semiclassical mechanics gives excellent agreement with experiments, at least when the trajectories are regular. Third, and most important, classical and semiclassical mechanics provide interpretation and insight that cannot easily be obtained from a quantum calculation.

In this paper, and in a subsequent one, we will show some results of semiclassical mechanics for the $m = 1$ energy eigenstates near $n = 30$ in magnetic fields of a few tesla and electric fields of a few hundred volts per centimeter.

II. QUANTUM PERTURBATION THEORY

The Hamiltonian for an electron in an atom which lies in static, uniform, collinear electric and magnetic fields is[5]

$$H = \frac{1}{2\mu} \left[\mathbf{p} + \frac{e\mathbf{A}}{c} \right]^2 - \frac{Ze^2}{r} - e\phi \ . \tag{1}$$

If the fields lie along the z axis, and F and B are the electric and magnetic field strengths, then

$$\mathbf{A} = \tfrac{1}{2}\mathbf{r} \times \mathbf{B} = \tfrac{1}{2}(\hat{\mathbf{i}}y - \hat{\mathbf{j}}x)B \ , \tag{2}$$

$$\phi = -Fz \ , \tag{3}$$

and it follows that

$$H = \frac{p^2}{2\mu} + \frac{eB}{2\mu c}L_z + \frac{e^2B^2}{8\mu c^2}(x^2 + y^2) - \frac{Ze^2}{r} + eFz \ . \tag{4}$$

The conventions involved in this equation are that $B > 0$ (or $F > 0$) means that $\mathbf{B}$ (or $\mathbf{F}$) is pointing in the $+z$ direction.

This Hamiltonian is invariant under rotations about the z axis, so L_z, the z component of the angular momentum, is a constant of the motion. The term linear in B in Eq. (4) leads to the Zeeman effect; this term, which is an additive constant, can be eliminated by transforming to a frame rotating about the z axis at the Larmor frequency, $eB/2\mu c$. The transformed Hamiltonian is[6(b)]

$$H = \frac{p^2}{2\mu} - \frac{Ze^2}{r} + \frac{e^2B^2}{8\mu c^2}(x^2 + y^2) + eFz \tag{5a}$$

$$= H_0 + \lambda H_1 + \nu H_2 \ , \tag{5b}$$

with

$$\lambda \equiv \frac{e^2B^2}{8\mu c^2}, \quad \nu \equiv eF \ , \tag{6a}$$

$$H_1 = x^2 + y^2, \quad H_2 = z \ . \tag{6b}$$

Equation (5) depends on B^2, so the eigenvalues (or the classical trajectories) do not depend upon the sign of B. The eigenvalues are also independent of the sign of F; if $\psi_F(x,y,z)$ is an eigenfunction of (5) having eigenvalue E_F,

then $\psi_F(x,y,-z)$ is an eigenfunction of $H_0 + \lambda H_1 - \nu H_2$ having the same eigenvalue, E_F.

For the field strengths we have studied, the Coulomb term in the Hamiltonian dominates, and the effects of the static fields may be calculated by first-order degenerate perturbation theory. The standard hydrogenic basis set may be used,

$$\Psi^{nmk}(r,\theta,\phi) = \sum_{l=|m|}^{n-1} C_l^{nmk} R_{nl}(r) Y_{lm}(\theta,\phi) \ , \tag{7}$$

where the expansion involves only the degenerate l levels at given n; m is an exact quantum number and n is a good quantum number in first order.

Our wave functions $R_{nl}(r)$ and $Y_{lm}(\theta,\phi)$ follow the phase conventions of Messiah.[7(a)] (The Y_{lm}'s are the same as those defined by Condon and Shortley,[7(b)] but the radial factors are different.) With these phase conventions, the required matrix elements can be calculated using the $L_\pm$ operators on the Y_{lm}'s and using the generating function for the R_{nl}'s. The result is

$$\langle nlm \mid z \mid nl'm \rangle = -\tfrac{3}{2} n [n^2 - (l+1)^2]^{1/2} \left[\frac{(l+m+1)(l-m+1)}{(2l+1)(2l+3)} \right]^{1/2}, \quad l'=l+1 \tag{8a}$$

$$= -\tfrac{3}{2} n (n^2 - l^2)^{1/2} \left[\frac{(l+m)(l-m)}{(2l-1)(2l+1)} \right]^{1/2}, \quad l'=l-1 \tag{8b}$$

$$\langle nlm \mid x^2+y^2 \mid nl'm \rangle = -\tfrac{5}{2} [n^2 - (l+2)^2]^{1/2} [n^2 - (l+1)^2]^{1/2} n^2$$

$$\times \left[\frac{(l+m+2)(l+m+1)(l-m+2)(l-m+1)}{(2l+5)(2l+3)^2(2l+1)} \right]^{1/2}, \quad l'=l+2 \tag{8c}$$

$$= \frac{n^2[5n^2+1-3l(l+1)](l^2+l-1+m^2)}{(2l-1)(2l+3)}, \quad l'=l \tag{8d}$$

$$= -\tfrac{5}{2} (n^2 - l^2)^{1/2} [n^2 - (l-1)^2]^{1/2} n^2$$

$$\times \left[\frac{(l+m)(l+m-1)(l-m)(l-m-1)}{(2l+1)(2l-1)^2(2l-3)} \right]^{1/2}, \quad l'=l-2 \ . \tag{8e}$$

Calculation of eigenfunctions and eigenvalues now involves diagonalization of a matrix of rank $(n - |m|)$, which for the interesting range of n's (~ 30) give accurate results with an insignificant amount of computer time. Results of such calculations will be shown later. While these calculations are very easy and quick, the resulting numbers by themselves do not provide much physical interpretation or insight. For example, we would like to know how the states divide themselves into families, and how the families change as the relative field strengths F and B change. For this purpose we find classical mechanics and especially classical perturbation theory to be helpful.

III. CLASSICAL PERTURBATION THEORY

A. The effective Hamiltonian

The unperturbed system is the Kepler problem in which the electron moves along a space-fixed elliptical path with the nucleus at one of the foci of the ellipse. When the fields are applied the electron is said to travel on a slowly evolving Kepler ellipse, with the plane of the orbit, the eccentricity, and the orientation of the ellipse continuously changing in time.

To apply canonical perturbation theory, the perturbed problem should be expressed in terms of the action and angle variables of the unperturbed motion. The angle variables ϕ_1, ϕ_2, and ϕ_3 are most easily understood by examining Fig. 1. In both left- and right-hand pictures of Fig. 1 the elliptical Kepler orbit and the plane of the orbit are embedded in a space-fixed Cartesian frame (X,Y,Z) whose origin is at the nucleus. Two vectors are shown. The vector with the canonical arrowhead is the angular momentum vector, **L**, which lies perpendicular to the orbital plane. The vector with the flat arrowhead labeled **A** in the right-hand picture is the Laplace or Runge-Lenz

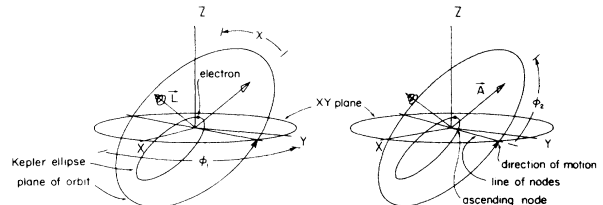
FIG. 1. A Kepler ellipse embedded in space-fixed Cartesian frame (X,Y,Z).

vector, which lies in the plane of the orbit and passes through the perihelion (or, more appropriately, the periapsis) of the Kepler ellipse. The orbital plane intersects the XY plane in the line of nodes, and the point where the electron passes from negative Z to positive Z is the ascending node. ϕ_1, the longitude of the ascending node, is the angle in the XY plane between the X axis and the line of nodes. ϕ_2, the argument of the perihelion, is the angle, measured in the orbital plane, between the line of nodes and the Laplace vector. ϕ_3, the mean anomaly, is the angular distance from perihelion of a point which rotates at constant angular velocity and which passes through the perihelion simultaneously with the actual moving electron. ϕ_3 is related by a complicated transcendental equation to the true anomaly, X, which is the angular distance between the instantaneous position of the electron and the Laplace vector.

The action variables of the Kepler problem are related to more familiar physical quantities. I_1 is the z component of the angular momentum; I_2 is the magnitude of the angular momentum vector, L; and I_3 is related to the total energy of the Kepler system. I_1, I_2, and I_3 correspond, respectively, to the quantum numbers m, l, and n of the quantum-mechanical Coulomb problem. The action and angle variables are summarized in Table I.

When the applied fields are nonzero, the action and angle variables change slowly in time, and the first-order approximation to the average change in these variables is found by averaging the canonical equations over one cycle τ of the unperturbed Kepler motion:

$$\frac{\Delta\phi_j}{\tau} = \frac{1}{\tau}\int_0^\tau \frac{\partial H}{\partial I_j}dt \qquad (9)$$

$$= \frac{\partial}{\partial I_j}\left[\frac{\lambda}{\tau}\int_0^\tau H_1 dt + \frac{\nu}{\tau}\int_0^\tau H_2 dt\right], \quad j=1,2 \qquad (10)$$

$$\frac{\Delta I_j}{\tau} = -\frac{1}{\tau}\int_0^\tau \frac{\partial H}{\partial \phi_j}dt \qquad (11)$$

$$= -\frac{\partial}{\partial\phi_j}\left[\frac{\lambda}{\tau}\int_0^\tau H_1 dt + \frac{\nu}{\tau}\int_0^\tau H_2 dt\right], \quad j=1,2,3 \ . \qquad (12)$$

Equations (9) and (10) hold because H_0 and τ depend only on I_3. Equation (10) does not hold for $j=3$, and the equation for $\Delta\phi_3/\tau$ is more complicated, but we will not use that equation. Equations (9) to (12) show that the *average* time development of I_1, I_2, I_3, ϕ_1, and ϕ_2 are given by canonical equations having the effective Hamiltonian

$$h = \frac{\lambda}{\tau}\int_0^\tau H_1 dt + \frac{\nu}{\tau}\int_0^\tau H_2 dt \ . \qquad (13)$$

The integrals are easy to evaluate (Appendix A) and when the nuclear charge $Z=1$, the result expressed in atomic units is

$$h = \frac{\lambda I_3^2}{4I_2^2}[(I_1^2+I_2^2)(5I_3^2-3I_2^2)$$

$$+ 5(I_3^2-I_2^2)(I_2^2-I_1^2)\cos(2\phi_2)]$$

$$- \frac{3\nu I_3}{2I_2}[(I_3^2-I_2^2)(I_2^2-I_1^2)]^{1/2}\sin\phi_2 \ . \qquad (14)$$

Differentiating h gives the average equations of motion for the I's and ϕ's.

The effective Hamiltonian (14) is independent of two of the angle variables. This is a remarkable simplification, which occurs for two quite different reasons. h is independent of ϕ_1 because the full Hamiltonian (5) has a symmetry: it is invariant under rotations about the z axis, and therefore L_z (alias I_1) is a constant of the motion. When H is written in I's and ϕ's, it is independent of ϕ_1, and this property, which must be retained in all orders of perturbation theory, is preserved in the first-order Hamil-

TABLE I. The action and angle variables of the Kepler problem.

$I_1=L_z$	Z component of the angular momentum vector. I_1 corresponds to the magnetic quantum number m of the quantum-mechanical Coulomb problem.
$I_2=\|\mathbf{L}\|$	Magnitude of the angular momentum vector. I_2 corresponds to total angular momentum quantum number l of the Coulomb problem. $I_2 \geq \|I_1\|$.
$I_3=(\mu k^2/-2H_0)^{1/2}$	The principal action, related to the Kepler energy H_0 and corresponding to the principal quantum number n of the Coulomb problem. $k=Ze^2$. $I_3 \geq I_2$.
ϕ_1	Longitude of the ascending node.
ϕ_2	Argument of the perihelion.
ϕ_3	Mean anomaly.

tonian, h. Equation (14) is independent of ϕ_3 because the full Hamiltonian has been averaged over a cycle of the Kepler motion and a cycle of the Kepler motion is nothing more than a cycle of ϕ_3. Independence of ϕ_3 is a property of first-order perturbation theory, whereas independence of ϕ_1 is a consequence of an exact symmetry of the problem.

When a Hamiltonian is independent of a coordinate, the corresponding momentum is a constant of the motion. For h, it follows that I_1 and I_3 are conserved quantities. (This is directly analogous to the fact that n and m are good quantum numbers in quantum perturbation theory.) In Eq. (14), therefore, I_1 and I_3 are reduced to the status of parameters. h is then a Hamiltonian for a one-dimensional problem with coordinate ϕ_2 and momentum I_2.

Yet another simplification results from the perturbation analysis. h has no explicit time dependence, and therefore it is conserved in first-order theory. Since the average evolution of I_2 and ϕ_2 is governed by equations of Hamiltonian form [(10) and (12)], it follows that I_2 and ϕ_2 must evolve on contours of h.

With this final simplification, the study of the effective Hamiltonian h is reduced to the study of a conservative, one-dimensional Hamiltonian system. The motions produced by the Hamiltonian h, and the evolution of these motions with changing electric and magnetic field, are best understood by sketching the energy contours, $h(I_2,\phi_2) = \text{const}$.

It is helpful to recall the energy contours for a simple pendulum, which has open curves corresponding to rotations, closed curves corresponding to librations, and stable and unstable fixed points (O points and X points). These structures and additional ones will arise in the present case.

A set of contour plots of $h(I_2,\phi_2)$ is shown in Fig. 2, for various values of v/λ. In every case we took $v < 0$ (so the electric field vector points toward $-z$). For $v > 0$ each figure would be reflected about $\phi_2 = \pi$.

B. Limiting cases

Before launching into the general case, we will examine the limits $F = 0$ or $B = 0$.

1. If there is a magnetic field but no electric field

If the electric field is absent, then the problem has been extensively studied by Delos, Knudson, and Noid,[6] Richards,[8(a)] and Robnik,[8(b)] (see also Braun and Solov'ev,[9(a)] and Herrick[9(b)]). Their work showed that both librations and rotations are present if the parameters I_1 and I_3 satisfy the inequality $I_1/I_3 < \sqrt{5}$, while only rotations exist when $I_1/I_3 > \sqrt{5}$.

In the absence of an electric field, the perturbation Hamiltonian is H_1 alone [see Eqs. (5) and (6)]; the corresponding effective Hamiltonian h_b is found by setting v to zero in Eq. (14):

$$h_b = \frac{\lambda I_3^2}{4I_2^2}[\,(I_1^2 + I_2^2)(5I_3^2 - 3I_2^2)$$

$$+ 5(I_3^2 - I_2^2)(I_2^2 - I_1^2)\cos(2\phi_2)]\,.\qquad(15)$$

Figure 2(a) is a contour plot of h_b calculated for $I_3 = 30$ and $I_1 = 1$. (We use atomic units, so $\hbar = 1$.) The ordinate of Fig. 2 is I_2 and the abscissa is ϕ_2. I_2 is never greater than I_3 or less than I_1. h_b is periodic in ϕ_2 with a period of π, and it is also symmetric about $\pi/2$. In the figure there are two classes of contour lines: closed loops centered on an O point at $\phi_2 = \pi/2$, $I_2 = 8.19$, and open curves which connect O to 2π. The motion around the loops is librational while that on the open curves is rotational. The motion on the loops is clockwise; the motion on the open curves is from 2π to 0. Also shown in Fig. 2 are two U-shaped separatrices which intersect the line $I_2 = 30$ at "T points." The T points are unstable fixed points, so motion on each separatrix has an infinite period.

In Ref. 6(b) it was explained how these two families of librators (here labeled L_A and L_C) and one family of rotors (labeled R) are connected to the quantum states of the system. Each trajectory (or contour) having an appropriately quantized value of the action variable (area within or under the contour) corresponds to a quantum state. It follows that (1) quantum states corresponding to librators are doubly degenerate and have low energies (a tiny splitting of the degeneracy results from tunneling); (2) quantum states corresponding to rotators are nondegenerate and have higher energies; and (3) energy gaps, which correspond to classical frequencies, are smallest for states closest to the separatrix. Additional details are given in Ref. 6(b). [This is the kind of interpretation that is difficult to obtain from quantum mechanics, but which falls out of the $h(I_2,\phi_2)$ contour plots.]

2. If there is an electric field but no magnetic field

The other limit of the theory, when the magnetic field is absent, leads to the Stark effect. This problem is separable in parabolic coordinates and the details of the quantum treatment can be found in Condon and Shortley.[7(b)] The first-order classical theory of the Stark effect was given by Born.[10] There is librational motion for all values of I_1 but there is never any rotational motion. For the Stark effect the perturbation Hamiltonian is H_2 [see Eqs. (6) to (8)]; the corresponding effective Hamiltonian h_e is found by setting λ to zero in Eq. (14),

$$h_e = -\frac{3vI_3}{2I_2}[(I_3^2 - I_2^2)(I_2^2 - I_1^2)]^{1/2}\sin\phi_2\,.\qquad(16)$$

Figure 2(h) is a contour plot of h_e calculated for $I_3 = 30$ and $I_1 = 1$. h_e is a periodic function of ϕ_2 with a period of 2π; it is antisymmetric about the line $\phi_2 = \pi$. Figure 2(h) has two sets of librators. One set (L_B) is confined to the region $0 \leq \phi_2 \leq \pi$, and (for $v < 0$) these librations have values of h_e greater than zero. The other set, L_A, a mirror image of the first, is confined to the region $\pi < \phi_2 \leq 2\pi$ and each member of this set has negative energy. A separatrix keeps the two sets of librators apart. This
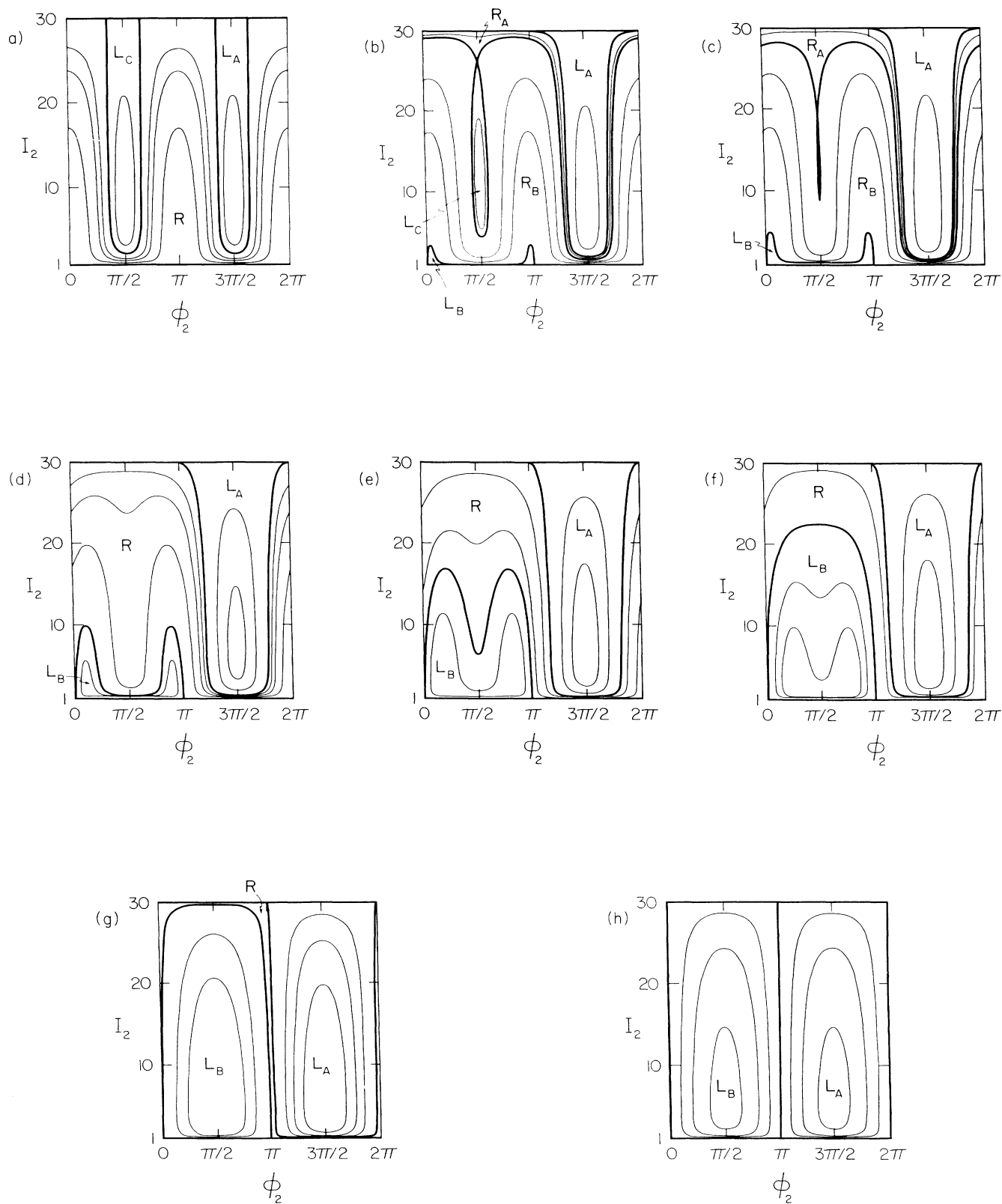
FIG. 2. Contour plots of $h(I_2,\phi_2)$ for parameter values $I_1=1$, $I_3=30$, and various values of $|v/\lambda|$. Always $v \le 0$. (a) $|v/\lambda|=0$, pure diamagnetic effect with no electric field; (b) $|v/\lambda|=300$; (c) $|v/\lambda|=450$; (d) $|v/\lambda|=900$; (e) $|v/\lambda|=1500$; (f) $|v/\lambda|=2000$; (g) $|v/\lambda|=10\,000$; (h) $|v/\lambda|=\infty$, pure Stark effect, with no magnetic field.

separatrix is the energy contour $h_e = 0$ which is the pair of rectangles formed by the five lines $I_2 = I_1$, $I_2 = I_3$, $\phi_2 = 0$, $\phi_2 = \pi$, and $\phi_2 = 2\pi$.

This separatrix has a very unusual property that was not mentioned by Born: It contains no fixed point. The only candidates are the points $I_2 = I_3$, $\phi_2 = n\pi$ and $I_2 = I_1$, $\phi_2 = n\pi$, but if one calculates the values of the derivatives at these points, $\dot{\phi}_2$ is not zero. The physical consequences of this unusual type of separatrix will be discussed later.

There are two O points, and these lie at the intersection of the lines $\phi_2 = \pi/2$, $\phi_2 = 3\pi/2$, and $I_2 = \sqrt{(I_1 I_3)}$. The period of the motion around every loop is the same. (As a consequence, the spacing between adjacent quantum energy levels is constant.)

C. The general case

The above examination of the limiting cases of the theory shows the complete difference between the diamagnetic interaction and the Stark effect. In either limit, the effective Hamiltonian is periodic in ϕ_2, but the periods differ by a factor of 2. The diamagnetic Hamiltonian is symmetric under reflection about the line $\phi_2 = \pi$ while the Stark Hamiltonian is antisymmetric. The diamagnetic motion includes both librations and rotations; the Stark motion is purely librational. Finally, there are unstable fixed points in the diamagnetic phase plane but there are none in the Stark phase plane.

Now, let us ask an interesting question. Suppose a highly excited hydrogen atom lies in a magnetic field of a few tesla. Classical mechanics tells us the genera and species of the motion: There will be librators here, rotators there, and so forth. Imagine now that the magnetic field is as before but there is a tiny electric field present as well. The contour lines of the Hamiltonian will be slightly different, but generally they will have changed in some smooth way. Make the electric field a little larger and the changes will be more noticeable but again the connection of the contour plot with the previous one will be clear. Keep repeating this process, and eventually, when the electric field dominates, the contour plot will evolve to the Stark limit. So, by following the evolution of contour plots for increasing values of the electric field strength, one can learn the qualitative properties of the motion at all relative field strengths. The development of contour plots for the parameter values $I_1 = 1$ and $I_3 = 30$ is shown in Figs. 2(a)—2(h).

The ratio $|v/\lambda|$ indicates the relative strength of the electric and magnetic field perturbations. From the definition of v and λ [Eqs. (6)] the units of v/λ are those of inverse length. In our calculations, we use atomic units for v/λ. To convert to laboratory units, if the magnetic field is B tesla, then given v/λ in atomic units the electric field strength in V/cm is approximately $F = 0.0117B^2(v/\lambda)$. When $|v/\lambda|$ is about n^2 (900 for this calculation), the electric and magnetic field contributions to the perturbation energy are comparable.

In Fig. 2(b) the electric field is small but nonzero and the contour plot differs somewhat from the pure magnetic field plot [Fig. 2(a)]. Three separatrices, shown as heavy

lines, separate five families of curves. There is a group of librators L_A restricted to $\pi \leq \phi_2 \leq 2\pi$ and another, smaller, group of librators L_C restricted to $0 \leq \phi_2 \leq \pi$. These two sets of librators evolved from the librators of Fig. 2(a). Notice also the peculiarly shaped separatrix that lies close to the $I_2 = 1$ line. A third class of librational motion exists inside this separatrix (though for this value of $|v/\lambda|$ the total area devoted to such motion is tiny). This set of librators has no analog in Fig. 2(a). The family of rotators R in Fig. 2(a) has bifurcated into two families, distinguishable by their behavior near $\pi/2$. One class, R_B, is confined to small values of I_2 near $\phi_2 = \pi/2$, that is, they dip below the set of librators on the left-hand side of the figure. The other class, R_A, is confined to large values of I_2 near $\phi_2 = \pi/2$; they pass above the librators.

In Fig. 2(c) the electric field is a little stronger and the main features of Fig. 2(b) remain. As in the previous figure, there are three separatrices. The L_C librators on the left-hand side of the figure are now restricted to a thin loop and the L_B librators near the $I_2 = 1$ line occupy a larger area. The L_A librators on the right-hand side of the figure and the two classes of rotators appear much as they did in Fig. 2(b).

Figure 2(d) is quite different from the previous two figures. There are two, not three, separatrices. The thin loop of Fig. 2(c) has disappeared and only two types of librational motion L_A and L_B remain. The librators restricted to $\pi < \phi_2 \leq 2\pi$ are still much as in Fig. 2(b), although the area devoted to these librators has grown steadily with increasing electric field. The librational motion near the $I_2 = 1$ line occupies a larger area and it now extends to larger values of I_2. Now there is nothing to distinguish R_A from R_B, so only one class of rotators, R, remains.

When the ratio $|v/\lambda|$ reaches 1500 [Fig. 2(e)] and then 2000 [Fig. 2(f)], the librators L_B occupy a large portion of the left-hand side of the figure. The area given over to the other type of librational motion is slowly increasing and the rotators are confined to a small region of the phase plane.

In Fig. 2(g) the electric field strength is large compared to the magnetic field strength. The two classes of librators occupy most of the (I_2, ϕ_2) plane and are increasingly coming to resemble one another. The separatrices appear to be approaching one another and the tiny gap between them is given over to rotational motion. The relationship of this figure to the Stark effect picture [Fig. 2(h)] is clear: As $B \rightarrow 0$, the two separatrices merge into the vertical lines dividing the two symmetric types of librational motion.

These pictures show the remarkable asymmetry in the evolution of the contour plots as one moves from the pure magnetic limit to the pure electric limit. The L_A librators on the right-hand side of Fig. 2(a) are connected to those on the right-hand side of Fig. 2(h), that is, they evolve in a smooth way from one limit to the other. The librators on the left-hand sides of Figs. 2(a) and 2(h) have no connection. The L_c librators of Fig. 2(a) disappear as the electric field increases. The positive energy L_B librators of Fig. 2(b) evolve out of the $I_2 = 1$ line and gradually grow

R. L. WATERLAND, J. B. DELOS, AND M. L. DU until they occupy the whole left half of Fig. 2(h).

The rotators of the diamagnetic effect also show interesting behavior. First, they split into two classes of rotors; then they become just one type again. Finally, they are squeezed between the two separatrices of Figs. 2(f) and 2(g) until they disappear.

D. Fixed points and separatrices

More detailed and quantitative information comes from the study of the movement of the fixed points of h as λ and ν change. The fixed points satisfy the equations

$$\dot{I}_2 = -\partial h / \partial \phi_2 = 0 ,$$
$$\dot{\phi}_2 = \partial h / \partial I_2 = 0 . \tag{17}$$

For the parameter values $I_1 = 1$, $I_3 = 30$, all fixed points lie on the line $\phi_2 = \pi/2$ or on the line $\phi_2 = 3\pi/2$.

For small values of the electric field there are three fixed points of h on the line $\phi_2 = \pi/2$. For tiny electric fields the I_2 value of one fixed point is very close to I_1 and the I_2 value of another is very close to I_3. The lower of these is an O point (stable) and the upper is an X point (unstable). The third fixed point is near $I_2 = 8.19$, which is the position of the O point for the diamagnetic problem. As the ratio $|\nu/\lambda|$ increases, the X point near I_3 decreases and the O point near 8.19 increases, and these fixed points approach one another. When the ratio is between 480 and 490, the two fixed points collide, and for larger electric fields neither exists. This is the critical value of $|\nu/\lambda|$ at which the separatrix dividing R_A and R_B disappears. Subsequently, there is only one fixed point which then remains for all larger values of the ratio $|\nu/\lambda|$. For very large values of $|\nu/\lambda|$ this fixed point approaches $(I_1 I_3)^{1/2}$, which is the position of the O point of the Stark problem.

For $\phi_2 = 3\pi/2$ there is one and only one fixed point for all values of $|\nu/\lambda|$. For small electric field this fixed point lies close to $I_2 = 8.19$. As the electric field increases, the I_2 value of the fixed point decreases, finally approaching the position of the O point of the Stark effect. The root is an O point.

Several other points in the diagram appear at first glance to be fixed points. Separatrices intersect the edge of the diagrams at $I_2 = I_1$ with $\phi_2 = 0$ or π, and $I_2 = I_3$ with $\phi_2 = \pi$ or 2π. Since X points are places where separatrices intersect, one might expect the above-mentioned points to be unstable fixed points.[11] In fact, however, $\dot{\phi}_2$ is nonzero at all of these points. This unusual behavior arises because of the nonanalytic form of h_e at $I_2 = I_1$ and $I_2 = I_3$.

Partly for this reason, the separatrices dividing L_A from R_A and L_B from R_B are less fundamental than the central separatrix dividing R_A, R_B, and L_C. Calculations of trajectories and wave functions in ρz space show that R_A, R_B, and L_C really represent distinct types of motion. However, in ρz space we cannot see any sharp distinction between L_A and R_A, or between R_B and L_B. As a consequence, we may legitimately categorize the families of trajectories in either of two ways. (1) We may say that there is a total of five or six families,

$$L_A, \ L_B, \ L_C, \ R_A, \ R_B ,$$

with R being the combined R_A and R_B after the distinction between them has disappeared. (2) We may say that there is a total of three or four families

$$A = L_A + R_A ,$$
$$B = L_B + R_B ,$$
$$C = L_C ,$$

with AB the combined A and B families after C has disappeared. These ways of categorizing the trajectories will be discussed further in connection with the correlation diagrams presented later.

IV. SEMICLASSICAL EIGENVALUES

A. Quantization rules

In Sec. III we used perturbation theory to replace a nonintegrable system with an integrable approximant. To find the energy spectrum, the classical dynamics of Sec. I must be quantized using the appropriate prescription. The classical equivalent of quantum eigenstates are a special set of trajectories called eigentrajectories, which correspond to discrete values of the action variables.[12] For the systems considered here, the appropriate discrete values are

$$I_1 = m \hbar , \tag{18}$$

$$I_3 = n \hbar , \tag{19}$$

$$A_2 = (2\pi)^{-1} \oint I_2 d\phi_2 = (k + \tfrac{1}{2}) \hbar . \tag{20}$$

Equations (18) and (19) are two of the quantization rules of the Kepler problem. We showed in Sec. I that the variables I_1 and I_3 are first-order constants of the motion and so it is reasonable that they should again be quantized as in the unperturbed problem.

The third quantization rule, Eq. (20), requires a great deal more thought. In the Kepler problem one of the conserved action variables is I_2, which corresponds to the length of the angular momentum vector $\mathbf{L}$. The semiclassical quantization rule for the unperturbed problem is

$$I_2 = |\mathbf{L}| = (l + \tfrac{1}{2}) \hbar .$$

However, when an electromagnetic field is present, the angular momentum vector changes in direction and magnitude, and the variable I_2 is not a constant of the motion. An action variable for the perturbed problem is defined as

$$A_2 = (2\pi)^{-1} \oint I_2 d\phi_2 ,$$

where the circular integral is over a cycle of the ϕ_2 motion.

While it is clear that A_2 is an action variable, and therefore a candidate for quantization, it is not obvious that half-integer values of A_2 correspond to quantum states. In fact, one might have guessed that the rule would involve full-integer quantization for rotators and half-integer quantization for librators. There are three ways to establish that (20) is the correct rule. (1) Compar-

TABLE II. Energy eigenvalues for $I_3 = 30\hbar$, $I_1 = 1\hbar$, and $v/\lambda = -300$. $B = 2$ T, $A_2 = (k + \frac{1}{2})\hbar$.

k	Quantized classical Type	perturbation theory Energy shift	Quantum perturbation theory Energy shift
0	L_A[a]	-2.3091[b]	-2.3047
1	L_A	-1.0365	-1.0319
2	L_A	0.1465	0.1508
3	L_A	1.2357	1.2398
4	L_A	2.2262	2.2299
5	L_A	3.1097	3.1128
23	R_A	3.8709	3.8726
0	L_C	4.3175	4.3146
22	R_A	4.4705	4.4675
20	R_B	4.7203	4.7491
19	R_B	5.0097	5.0168
18	R_B	5.3631	5.3723
17	R_B	5.7703	5.7787
16	R_B	6.2259	6.2343
15	R_B	6.7272	6.7355
14	R_B	7.2720	7.2804
13	R_B	7.8590	7.8674
12	R_B	8.4870	8.4954
11	R_B	9.1552	9.1637
10	R_B	9.8631	9.8716
9	R_B	10.6102	10.6186
8	R_B	11.3958	11.4043
7	R_B	12.2198	12.2284
6	R_B	13.0820	13.0906
5	R_B	13.9820	13.9906
4	R_B	14.9198	14.9284
3	R_B	15.8950	15.9037
2	R_B	16.9077	16.9164
1	R_B	17.9578	17.9663

[a]For this value of v/λ, there are two types of librator (labeled L_A and L_C) and two types of rotator (labeled R_A and R_B).

[b]Energy shift in units of 10^{-6} hartree (1 hartree $= 219\,474.63$ cm^{-1}).

ison of semiclassical eigenvalues with those calculated by quantum perturbation theory shows that half-integral quantization is appropriate for all states, and that full-integral quantization leads to poor results for the rotators. (2) A rigorous proof comes from the Einstein-Brillouin-Keller-Maslov semiclassical framework.[12,13] In this framework, a semiclassical approximation to the wave function is derived in ordinary coordinates (Cartesian or cylindrical, etc., not action-angle coordinates). An action variable such as A_2 is expressed as an integral around a path lying on a smooth surface in phase space. Singular regions on this surface are identified, and each singular region through which the path passes produces an additional phase shift described by a quantity called the Maslov index μ. Then the quantization condition is given as $A = (k + \mu/4)\hbar$. In Ref. 6(b), it was shown for the case $v = 0$ that the paths involved in the evaluation of A_2 always pass through two singular regions, and the Maslov index μ is equal to 2. Calculations show that this still holds if v is nonzero. Therefore, Eq. (20) is the appropriate condition. (3) Since h is expressed in terms of action-angle variables, it would be interesting to obtain a proof of Eq. (20) that remains entirely within the action-angle formation, and does not refer back to Cartesian coordinates.
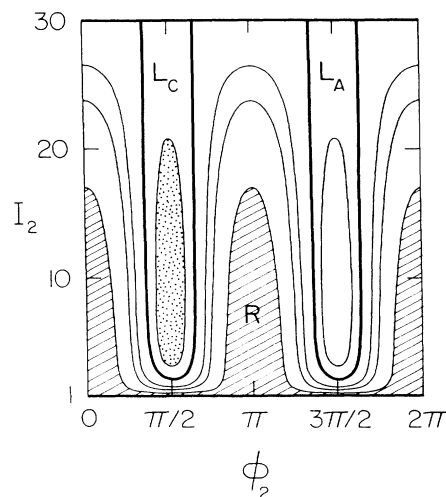

FIG. 3. For a rotating state, A_2 is related to the area between a contour curve and the $I_2 = 0$ line (striped area). Not shown in this figure is the rectangular strip between the $I_2 = 1$ and $I_2 = 0$ lines. This strip contributes an additional 2π units to the area. For a librating state, A_2 is related to the area closed by a loop (dotted area).

TABLE III. Eigenfunctions and eigentrajectories shown in Figs. 9 and 10.

	Type	k quantum number	$\lvert v/\lambda \rvert$	Energy level[a]
(a)	L_A	4	400	5
(b)	R_A	21	400	9
(c)	R_B	12	400	18
(d)	R_B	1	100	29
(e)	R	15	3000	15
(f)	L_B	8	3000	21
(g)	L_C	2	100	8
(h)	Mixed		400	10

[a]If the energy shifts for all 29 states at $I_3 = 30$, $I_1 = 1$ with fixed v/λ are listed in order with number one being the lowest or most negative and number 29 being the highest, then this label identifies the state.

Recently, we have obtained such a proof, and it will be published in a future paper.

Irrespective of the complications involved in a rigorous proof of Eq. (20), implementation of this rule is very simple. A_2 is related to an area in the contour plots of Sec. III. For a librator, A_2 is $1/2\pi$ times the area enclosed by the loop, while for a rotator, A_2 is $1/2\pi$ times the area enclosed between the contour line of the rotator and the $I_2 = 0$ line (Fig. 3). For the librators, k ranges from zero to some maximum (typically ~ 5, and always much less than $n - \lvert m \rvert$), while for the rotators, k ranges from m to a maximum which is close to $n - \lvert m \rvert$ minus the number of librators. These areas were calculated numerically, and Newton's method gave the eigenvalues.

B. An energy spectrum for $n = 30$ and $m = 1$

Fixing two of the parameters in the Hamiltonian (14) to $I_1 = 1$, $I_3 = 30$, we have calculated the energy spectrum for a range of values of $\lvert v/\lambda \rvert$. Table II shows an example of our results for $\lvert v/\lambda \rvert = 300$ (or, equivalently, $n = 30$, $m = 1$, $B = 2$ T, and $F = -14$ V/cm). The eigenstates are labeled by their type [see Fig. 2(b) for the definition of types of state] and by their A_2 quantum number k.

Also shown in this table are the results of first-order degenerate quantum perturbation theory. The tabulated values agree to two or three significant figures. In general for any value of v/λ, the agreement is two or three figures. The semiclassical results are least accurate for motion near a separatrix and for nearly degenerate states: Quantum-mechanical tunneling is important for such states and the semiclassical theory we have used does not take tunneling into account.

In the contour plots of Sec. II, I_2 can range between I_1 and I_3 while ϕ_2 has a range of 2π. The total area available for motion is, therefore, $2\pi(n - \lvert m \rvert)\hbar$ where I_1 and I_3 have been replaced by their quantized values. One sees directly that the maximum value of A_2 is $(n - \lvert m \rvert)\hbar$ and so one expects to find $(n - \lvert m \rvert)$ quantum states. For our calculations $(n - m)$ is 29 and indeed Table II contains 29 eigenvalues. There was one parameter value (when $\lvert v/\lambda \rvert = 400$) for which we could find only 28 semiclassical eigenvalues. The missing state lies very close to the separatrix between R_A and R_B rotating states. As mentioned above, states close to a separatrix are subject to quantum-mechanical tunneling effects and since this theory neglects all such effects we cannot find or categorize the missing state.

C. Correlation diagram connecting the states of the diamagnetic effect to those of the Stark effect

The best way to present the results of this calculation is to construct a correlation diagram. With I_1 and I_3 fixed, the effective Hamiltonian still contains two parameters, λ and v, but if we write

$$h = \lambda(h_b + v/\lambda h_e) ,$$

then for any fixed value of v/λ the eigenvalues are linear functions of λ (in first-order perturbation theory). Hence only the dependence of v/λ is interesting. For $v = 0$, the value $\lambda = 9.06 \times 10^{-12} \equiv \lambda_0$, which corresponds to $B = 2$ T, produces a reasonable splitting of eigenvalues, the largest of which is 1.04274×10^{-6} hartrees. On the other hand, if $\lambda = 0$, the Stark effect (for which the eigenvalues are known analytically) produces a comparable splitting if $v = 8.28 \times 10^{-10} \equiv v_0$ which corresponds to $F = 4.25$ V/cm. In the (v, λ) plane (Fig. 4) we may draw a straight line from $(0, \lambda_0)$ to $(v_0, 0)$, and compute the eigenvalues as functions of v/λ at a set of points on this line. Since the eigenvalues change linearly on any line through the origin, it follows that determining the eigenvalues on the specified line determines them everywhere in the plane (to first order).

In Figs. 5 and 6 we have plotted the energy eigenvalues obtained from quantized classical perturbation theory on a graph with $\log_{10}\lvert v/\lambda \rvert$ as abscissa and energy as ordinate. This produces a set of points arranged on lines of constant $\lvert v/\lambda \rvert$. What we gained by doing the classical perturbation theory is a way to categorize the states: Each state is unambiguously labeled by its type $(L_A, L_B, R_A,$ etc.) and the value of its A_2 quantum number. States of the same type and the same quantum number should therefore be connected. Figure 5 shows the evolution of the eigenvalues with increasing electric field for $\lvert v/\lambda \rvert$ values from 1 to 10^6. Figure 6 shows a smaller range of $\lvert v/\lambda \rvert$ (100 to 1000). In both figures lines con-
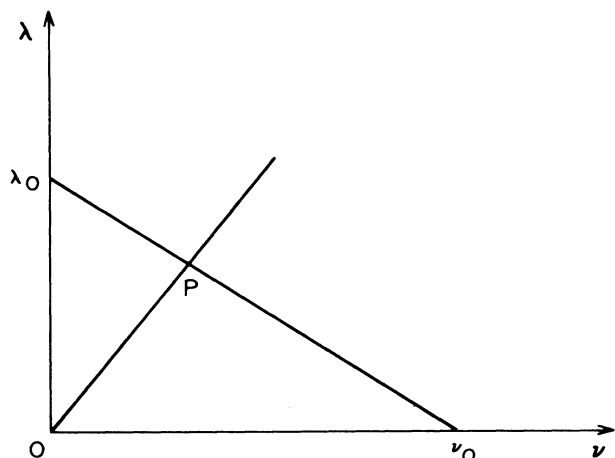
FIG. 4. The correlation diagram is constructed by calculating energy levels along a straight line in the (ν,λ) plane from $(0,\lambda_0)$ to $(\nu_0,0)$. On a line through the origin the eigenvalues change linearly.

FIG. 6. The portion of Fig. 5 from $\log_{10}(\nu/\lambda)=2$ to 3.

nect states of the same type and the same A_2 quantum number: Solid lines connect L_A librators; short dashed lines connect L_C librators; long dashed lines connect L_B librators; the dotted lines connect L_C librators; the dotted lines connect R_B rotating states; and the open circles are R_A rotators.

The most interesting aspect of the correlation diagram is the different ways of thinking about it in classical mechanics and in quantum mechanics. In quantum

FIG. 5. A correlation diagram connecting the states of the diamagnetic effect (left-hand side of the figure) to those of the Stark effect (right-hand side of the figure). The boxed regions are shown on an expanded scale in Figs. 6 and 8.
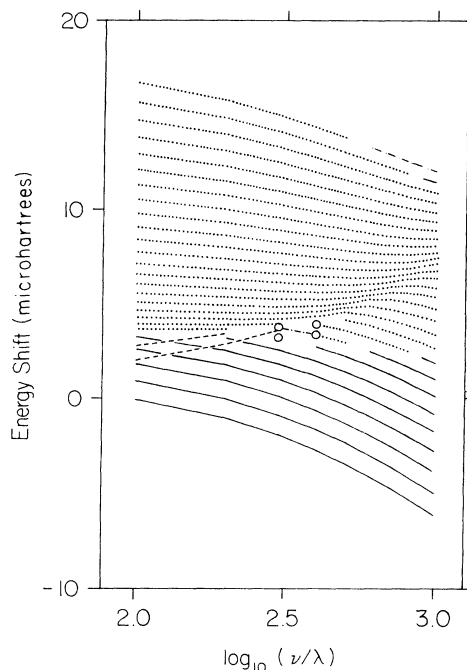
mechanics we know that the total number of states is preserved, and we think of the states adjusting continuously as the field strengths change. In most cases the change of the eigenstate with changing fields is very gradual. Where Figs. 5 and 6 show crossings, we know that the correlation can be made adiabatically, preserving the order of energy levels, or diabatically, preserving the character of the states.

In classical mechanics, however, eigentrajectories of a given character actually disappear suddenly and eigentrajectories of different character appear equally suddenly. Furthermore, the point at which one eigentrajectory disappears is not necessarily the same as the point at which some other eigentrajectory appears to take its place. Hence semiclassical mechanics permits breaks in the diagram. We already mentioned that at $|\nu/\lambda|=400$ there is a "missing" semiclassical state. For similar reasons, at $|\nu/\lambda|=300$ there is an "isolated" R_A state having $k=23$.

While quantum mechanics predicts that these states must be continuously connected to nearby states, semiclassical mechanics tell us that the changes of character of the states must become increasingly abrupt in the limit $\hbar\rightarrow 0$.

More detailed properties of the correlation diagram follow. (1) The degenerate states of the diamagnetic effect are split linearly by the Stark effect for small electric field but the nondegenerate states experience a quadratic Stark effect. (2) As the electric field increases from zero, the L_C librators disappear one by one, and they are replaced by R_A and R_B rotators. (3) At the critical value of $|\nu/\lambda|$ (about 480) the L_C motion disappears and the R_A and R_B rotator states are no longer distinct. (4) The R_A rotors only exist in a small range of $|\nu/\lambda|$ values (approximately 300 to 400). (5) There is an isolated R_A state

with a quantum number $k = 23$ at $v/\lambda = 300$. This state persists over only a very small range of $|v/\lambda|$. (6) Rotating states are gradually displaced by L_A and L_B librating states as $|v/\lambda|$ becomes large. One rotor remains at the last plotted value of $\log_{10}|v/\lambda|$. (7) For very large $|v/\lambda|$ the states are equally spaced, as is characteristic of the degenerate Stark effect. (8) The highest energy states are classified R for $v/\lambda = 0$; they then become R_B, then at large $|v/\lambda|$ they become L_B. However, there appears to be no abrupt change in character of the states.

The last of these observations reemphasizes the point made earlier, that there does not appear to be much difference between L_B and R_B (or between L_A and R_A). The separatrices with fixed points divide distinct types of motion, but separatrices without fixed points do not. A qualitative picture describing the development of these families of states is shown in Fig. 7.

V. EIGENFUNCTIONS AND EIGENTRAJECTORIES

Plots of eigenfunctions and eigentrajectories provide another way of understanding the structure of the various rotators and librators. The eigenfunctions were calculated by first-order perturbation theory, as in Sec. II. Corresponding eigentrajectories were calculated by selecting ar-

FIG. 7. Qualitative picture of the development of families of states with changing fields. At $|v/\lambda| = 0$, L_A and L_C are degenerate. There is a very tiny splitting between symmetric and antisymmetric linear combinations of L_A and L_C states; we have denoted the resulting families L_+ and L_-. With very small electric field these states unscramble themselves into L_A and L_C. As the electric field increases, the L_C or C states increase in energy, while the lowest R's and the L_A's go to R_A and L_A, or A states. The higher R's go to R_B and L_B, or B states. So long as the C states exist, there is a fundamental distinction between A and B states, but the differences between R_A and L_A or R_B and L_B are not very great. When the field is still stronger, the C states disappear, and with them the clear distinction between A and B states. The combined family might be called type AB, or it could be subdivided into L_A, R, and L_B.

bitrary initial values $\phi_1 = 0$, $\phi_2 =$ either $\pi/2$ or $3\pi/2$, $\phi_3 = 0$, $I_1 = 1$, $I_3 = 30$, and I_2 equal to the value taken on the appropriate quantized curve in the plots in Fig. 2 at the chosen initial value of ϕ_2. Then these values were translated into corresponding initial values of ρ, z, p_ρ, p_z using the formulas in Appendix B. The trajectory was then computed and plotted using the exact equations of motion (which in ρz coordinates are simpler than the first-order equations).

A representative set of eigentrajectories and eigenfunctions is shown in Figs. 9 and 10. Figure 8 shows points on the correlation diagram corresponding to these states. The selected states are listed in Table III. In all cases, one sees that the wave function is large in the region of ρz space occupied by the eigentrajectory, and small elsewhere. For rotators, the quantum number k is equal to the number of crests in the eigenfunction on an appropriate curve. For librators, this quantum number is one less than the number of crests on some curve.

State (a) is type L_A. With ϕ_2 always close to $3\pi/2$, the periapsis tends to stay close to the negative z axis, and the Kepler ellipse stretches out toward positive z. The electron therefore spends most of its time at moderate ρ and positive z. The eigenfunction has five crests in the ρ direction, one more than the quantum number $k = 4$.

State (b) is type R_A. It has fundamentally the same structure as (a), showing again that there is not much difference between L_A and R_A states. The k quantum number for this rotator is 21; it counts the number of crests going around the curved boundary of the trajectory. This eigenfunction also contains an interesting ridge that corresponds to a "swallowtail" structure in the trajectory.[14]
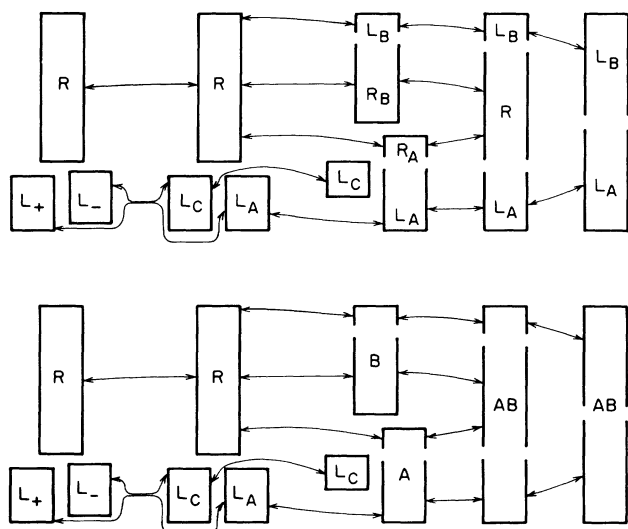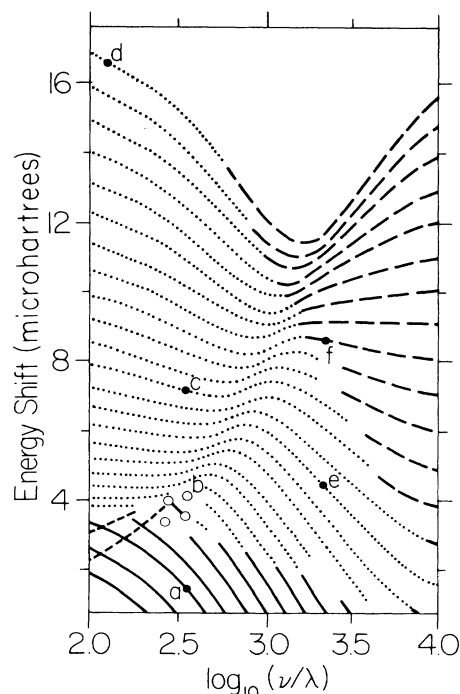

FIG. 8. Points on the correlation diagram for which eigentrajectories and eigenfunctions are shown in Figs. 9 and 10.

State (c) is a typical R_B. If the electric field were zero, then the trajectory and the probability density would be symmetric about the z axis. As the electric field is turned on, the state is slightly distorted, and the energy shows a quadratic Stark effect.

State (d) is an extreme R_B. If there were no electric field, there would be a periodic orbit lying on the ρ axis. With the electric field, that orbit is somewhat distorted. The eigentrajectory undergoes small stable oscillations about this periodic orbit. With $k = 1$, almost all of the action is associated with motion in ρ, and if we move along a line $\rho =$ const, we encounter just one crest. This is the highest-energy state.

State (e) is of type R, at a large $|\nu/\lambda|$ such that the separatrix dividing R_A from R_B has disappeared. This state is nearly symmetric about the z axis, and when B

goes to zero it correlates to the center Stark state with zero energy shift.

State (f) is a typical L_B. It is very similar in structure to state (e), showing the continuous change of (ρz) trajectories across the R-L_B separatrix. Its k quantum number is 8, which is one less than the number of crests on the curved boundary.

State (g) is an L_C. Having ϕ_2 always close to $\pi/2$, the Kepler ellipse reaches out along the $-z$ axis, and the electron spends most of its time in that region. The Stark effect for this state is linear, and the energy shift is positive for $\nu < 0$. In this case $k = 2$, one less than the number of crests encountered on a line of constant negative z. Perhaps just barely visible in this wave function is some amplitude in the classically forbidden region at positive z.

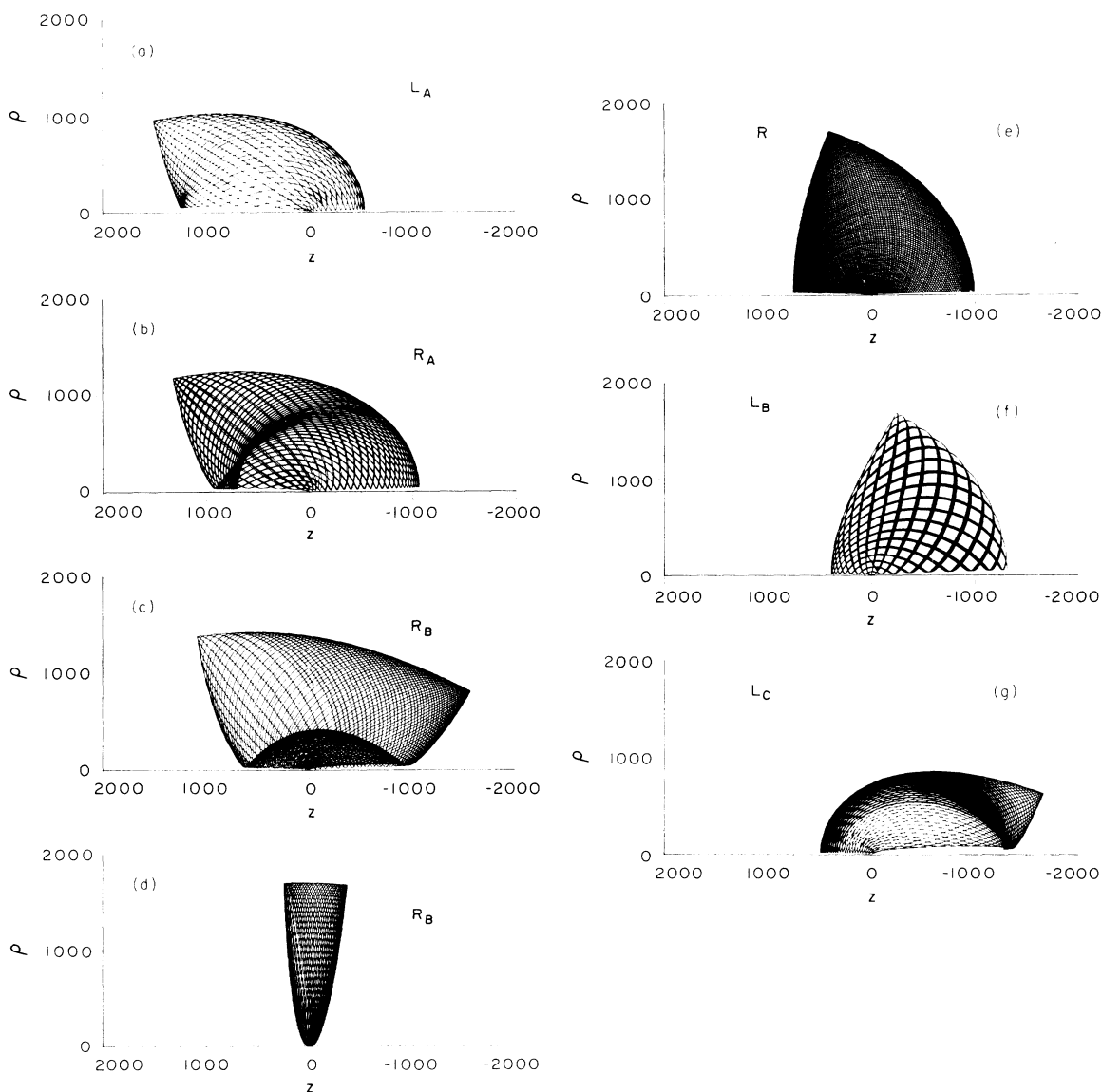State (h) has mixed character. This is the "missing

FIG. 9. Selected eigentrajectories (trajectories with appropriately quantized action variables).

state." There exists no trajectory having half-integral A_2 that corresponds to this state. We see that the probability density is largest in a region similar to that occupied by L_C states, but there is also some amplitude in regions occupied by R_A or R_B states. A semiclassical description of this state must incorporate tunneling effects.

VI. COMPARISON WITH EXPERIMENTS AND WITH OTHER THEORETICAL FORMULATIONS

Presently there exist no measurements on $m = 1$ states. There is an interesting paper by Braun and Solov'ev[15] which describes the combined Stark-Zeeman effect if the
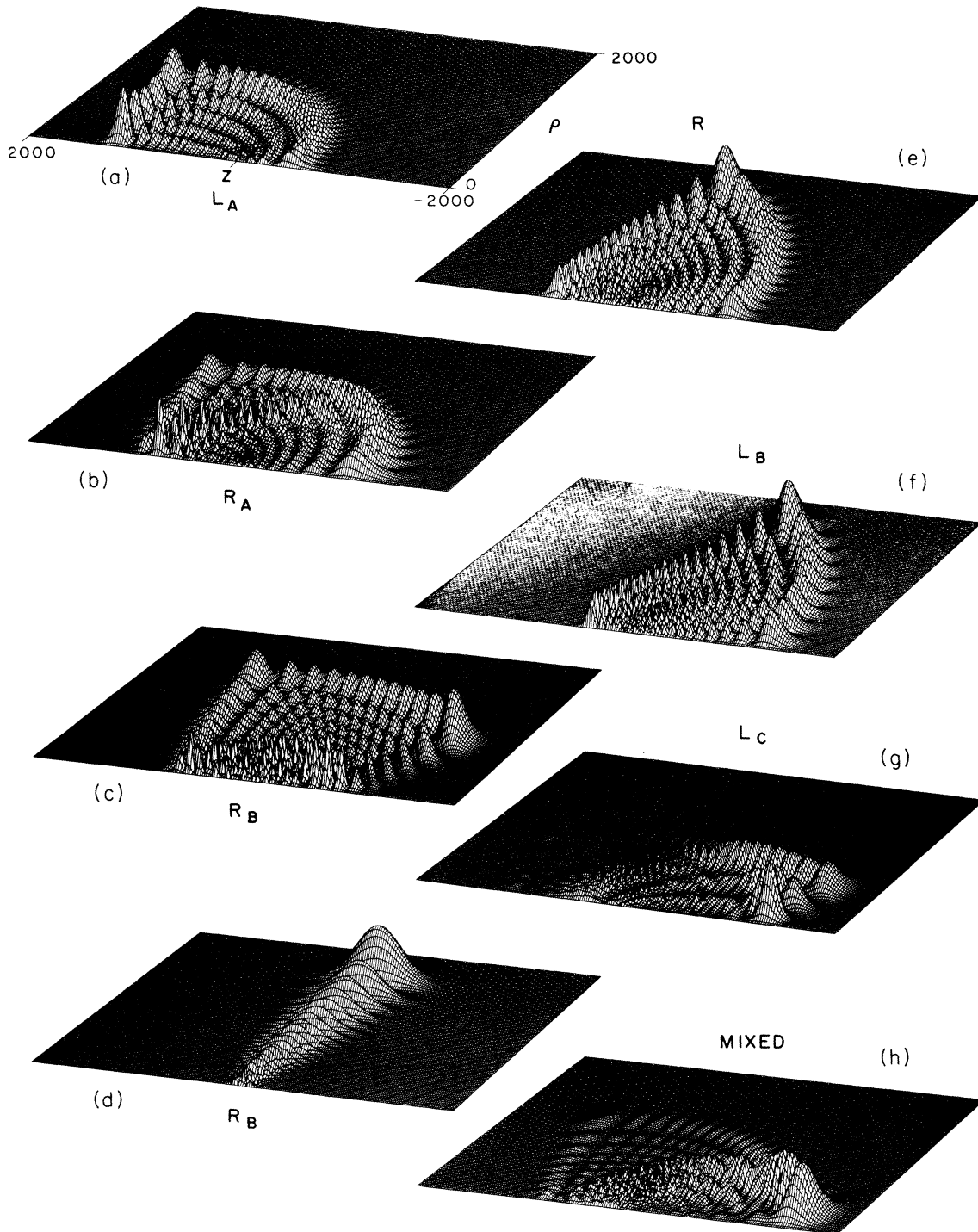
FIG. 10. Selected eigenfunctions corresponding to eigentrajectories in Fig. 9.

effect of the electric field is much less than that of the magnetic field (small $|v/\lambda|$).

After this work was mostly complete, Cacciani et al. reported an experimental determination of the energy spectrum of highly excited lithium atoms which lie in parallel electric and magnetic fields.[16] They also calculated the energy spectrum of $n = 30$, $m = 0$ hydrogen atoms for a range of electric fields and a fixed magnetic field of 2.33 T.

Cacciani et al. used a semiclassical theory first derived by Solov'ev[15] to show that the classical dynamics of an electron in parallel electric and magnetic fields has an approximate constant of the motion which they labeled Λ_β. Λ_β is related to the Laplace vector $\mathbf{A}$ by the expression

$$\Lambda_\beta = 4A^2 - 5(A_z - \beta)^2 + 5\beta^2 ,$$

where $\beta = 2.4f/(n\gamma)^2$, $f = F/(5.142 \times 10^9 \text{ V/cm})$, and $\gamma = B/(2.35 \times 10^5 \text{ T})$. The parameter β measures the relative strength of the electric and magnetic field strengths. β is the counterpart in Solov'ev's theory of our parameter $|v/\lambda|$. Solov'ev's theory is, in fact, formally equivalent to quantized first-order classical mechanics. In particular, if we calculated the energy spectrum for the parameter values $n = 30$ and $m = 0$, the results would be exactly the same as those of Cacianni et al. For this reason we have not calculated the energy spectrum for $n = 30$ and $m = 0$ but we have found an alternative explanation of two criteria first found by Braun and Solov'ev[15] and restated by Cacciani et al.[16]

For $m = 0$ there are three types of states, which Cacciani et al. labeled I, II, and III. As the electric field F (or, equivalently, β) increases, the type II states begin one by one to disappear. When $\beta = \frac{1}{5}$, the complete class II has disappeared. As the electric field increases further, class III begins to disappear and for β greater than 1 only class I remains. If one translates these criteria ($\beta = \frac{1}{5}$ and 1) into criteria for v/λ, the result is $|v/\lambda| = 600$ and 3000. These v/λ criteria are directly related to the disappearance of fixed points in the (I_2, ϕ_2) pictures. To see this, one must perform the fixed point analysis for m (alias $I_1) = 0$ which, in contrast to the $m = 1$ case, can be examined analytically.

When $I_1 = 0$, the effective Hamiltonian (14) is

$$h = \frac{\lambda I_3^2}{4}[(5I_3^2 - 3I_2^2) + 5(I_3^2 - I_2^2)\cos(2\phi_2)]$$

$$- \frac{3vI_3}{2}(I_3^2 - I_2^2)^{1/2}\sin\phi_2 . \qquad (21)$$

Straightforward analysis shows the following: (1) There is a fixed point at $\phi_2 = \pi/2$, $I_2 = 0$, which exists for all values of v/λ. (2) for $v/\lambda < 0$, there is a fixed point at $\phi_2 = \pi/2$, and

$$I_2 = \left[I_3^2 - \frac{9}{4}\left[\frac{v}{\lambda}\right]^2 \frac{1}{I_3^2}\right]^{1/2} ,$$

provided that $|v/\lambda|$ is not too large. In fact, this fixed point collides with the first one and disappears when

$$\left|\frac{v}{\lambda}\right| = \frac{2}{3}I_3^2 .$$

If I_3 (alias n) is 30, the critical value equals 600, which is the criterion of Cacciani et al. for the disappearance of "type II" states. For $v/\lambda > 0$, this fixed point occurs at $\phi_2 = 3\pi/2$, and it disappears under the same condition. (3) There is a fixed point at $I_2 = 0$, with ϕ_2 such that

$$\sin\phi_2 = \frac{3}{10}\frac{v}{\lambda}\frac{1}{I_3^2} ,$$

again provided v/λ is not too large. This fixed point disappears when the magnitude of the right-hand side exceeds unity, or

$$\left|\frac{v}{\lambda}\right| = \frac{10}{3}I_3^2 .$$

When $I_3 = 30$, this second critical value of v/λ is 3000, which is the criterion for disappearance of "type III" states. Thus the disappearance of families of states again corresponds to the disappearance of fixed points in the $h(I_2, \phi_2)$ plots.

VII. CONCLUSION

We have presented a semiclassical calculation of the energy spectrum of an $n = 30$, $m = 1$ atom in parallel electric and magnetic fields. All semiclassical theories begin with the solution of classical equations of motion and end with the quantization of the adiabatic invariants of the classical theory. We solved the first-order classical perturbation theory equations of motion and quantized the classical action variables using the Einstein-Brillouin-Keller-Maslov quantization rule.

This semiclassical analysis, and especially the contour plots of $h(I_2, \phi_2)$, provide interpretation and insight that cannot easily be obtained by other means. Through these pictures the trajectories and their associated quantum states are sorted into families. The development of these families with changing field strengths is summarized in the correlation diagrams, Figs. 5–7.

APPENDIX A: EVALUATION
OF EFFECTIVE HAMILTONIAN

The diamagnetic contribution to the effective Hamiltonian was given in Ref. 6(b). There were several misprints, which are corrected below.

The equations above Eq. (A8) of Ref. 6(b) should be

$$\cos^2\phi_2 = \tfrac{1}{2}[1+\cos(2\phi_2)] ,$$

$$\sin^2\phi_2 = \tfrac{1}{2}[1-\cos(2\phi_2)] .$$

The equations below (A9) should be

$$r = a(1-e\cos\psi) ,$$

$$\frac{dt}{d\psi} = \frac{\tau}{2\pi}(1-e\cos\psi) ,$$

and (A12) should be

$$\lambda\overline{H}_1 = \lambda a^2[(1+\tfrac{3}{2}e^2)(\tfrac{1}{2})(1+\cos^2 i)$$
$$+\tfrac{5}{2}e^2\tfrac{1}{2}(1-\cos^2 i)\cos 2\phi_2] .$$

The method given there can also be used to find the electric contribution to h. In a frame of reference such that the orbit lies in the $x''y''$ plane, with the positive x axis corresponding to the periapsis, averaging over one Kepler cycle gives

$$\overline{y}'' = 0 ,$$

$$\overline{z}'' = 0 ,$$

and

$$\overline{x}'' = \frac{1}{\tau}\int_0^\tau x''(t)dt$$
$$= \frac{1}{\tau}\int_0^\tau r(t)\cos\chi(t)dt . \qquad \text{(A1)}$$

Converting again to ψ as the independent variable,

$$\overline{x}'' = \frac{1}{\tau}\int_0^{2\pi} a(1-e\cos\psi)(\cos\psi-e)\left[\frac{\tau}{2\pi}\right]d\psi$$

$$= -\tfrac{3}{2}ae . \qquad \text{(A2)}$$

The contribution to h coming from the electric field is

$$h = v\overline{z} , \qquad \text{(A3)}$$

with z referred to the space-fixed frame. Elements of a given vector referred to the space-fixed frame are related to its elements in the rotated frame by

$$\begin{bmatrix} \overline{x} \\ \overline{y} \\ \overline{z} \end{bmatrix} = A^\dagger \begin{bmatrix} \overline{x}'' \\ \overline{y}'' \\ \overline{z}'' \end{bmatrix} , \qquad \text{(A4)}$$

where A is the rotation matrix $\underline{A} = A_{iii}A_{ii}$ given in Eq. (A5) of Ref. 6(b). Hence

$$\overline{z} = A_{zx}^\dagger \overline{x}''$$

$$= \overline{x}'' \sin\phi_2\sin i$$

$$= -\tfrac{3}{2}ae \sin i \sin\phi_2 . \qquad \text{(A5)}$$

Finally, since $a = I_3^2/\mu k$, $\sin i = (1-I_1^2/I_2^2)^{1/2}$, and $e = (1-I_2^2/I_3^2)^{1/2}$, we obtain Eq. (14) for h.

APPENDIX B: CONVERSIONS BETWEEN CARTESIAN AND KEPLER ACTION-ANGLE VARIABLES

Kepler action-angle variables are defined and described in Ref. 6(b). Here we give an algorithm for converting into and out of these variables. Conventions in the equations below are that all angles vary between $-\pi$ and π, except for i, which varies between 0 and π. All square roots are positive unless otherwise noted.

1. Action-angle to Cartesian

Suppose we are given values of the action-angle variables $\{I_i,\phi_i\}$, and we wish to find the position and velocity of the electron.

(1) Evaluate the eccentricity of the orbit

$$e = (1-I_2^2/I_3^2)^{1/2} . \qquad \text{(B1)}$$

(2) Evaluate the "eccentric anomaly" ψ by numerically solving the transcendental equation

$$\phi_3 = \psi-e\sin\psi . \qquad \text{(B2)}$$

If $\phi_3 = 0$ or $\pm\pi$, then $\psi = 0$ or $\pm\pi$, respectively.

(3) Evaluate the "true anomaly" χ (the angle in the plane of the orbit between the electron and the periapsis) using

$$\tan(\tfrac{1}{2}\chi) = \left[\frac{1+e}{1-e}\right]^{1/2}\tan(\tfrac{1}{2}\psi) . \qquad \text{(B3)}$$

Again if $\phi_3 = 0$ or $\pm\pi$, then $\chi = 0$ or $\pm\pi$, respectively.

(4) Evaluate the distance of the electron from the nucleus r using the orbit equation

$$\frac{1}{r} = \frac{\mu k}{I_2^2}(1+e\cos\chi) . \qquad \text{(B4)}$$

(5) Evaluate the Kepler energy

$$H_K = -\mu k/2I_3^2 \qquad \text{(B5)}$$

and then evaluate the radial momentum

$$p_r = \left[2\mu\left[H_K-\frac{I_2^2}{2\mu r^2}+\frac{k}{r}\right]\right]^{1/2} \qquad \text{(B6)}$$

with the sign of p_r the same as the sign of χ. The radial momentum also vanishes if $\chi = 0$ or $\pm\pi$. The tangential component of the momentum is

$$p_T = I_2/r . \qquad \text{(B7)}$$

(6) Evaluate the Cartesian position and momentum of the particle in the plane of the orbit using

$$x''' = r\cos\chi ,$$

$$y''' = r\sin\chi ,$$

$$z''' = 0 ,$$

$$p_x''' = p_r\cos\chi - p_T\sin\chi , \qquad \text{(B8)}$$

$$p_y''' = p_r\sin\chi + p_T\cos\chi ,$$

$$p_z''' = 0 .$$

(7) Rotate these vectors into space-fixed coordinates using

$$\begin{bmatrix} x \\ y \\ z \end{bmatrix} = A^T \begin{bmatrix} x''' \\ y''' \\ 0 \end{bmatrix} ,$$

$$\begin{bmatrix} p_x \\ p_y \\ p_z \end{bmatrix} = A^T \begin{bmatrix} p_x''' \\ p_y''' \\ 0 \end{bmatrix} ,$$

(B9)

where A^T is the transpose of the matrix A, and A is the product of three rotations

$$A = A_3 A_2 A_1 , \tag{B10}$$

$$A_1 = \begin{bmatrix} \cos\phi_1 & \sin\phi_1 & 0 \\ -\sin\phi_1 & \cos\phi_1 & 0 \\ 0 & 0 & 1 \end{bmatrix} , \tag{B11a}$$

$$A_2 = \begin{bmatrix} 1 & 0 & 0 \\ 0 & \cos i & \sin i \\ 0 & -\sin i & \cos i \end{bmatrix} , \tag{B11b}$$

$$A_3 = \begin{bmatrix} \cos\phi_2 & \sin\phi_2 & 0 \\ -\sin\phi_2 & \cos\phi_2 & 0 \\ 0 & 0 & 1 \end{bmatrix} . \tag{B11c}$$

The formula is simplified in the obvious way if $\phi_1 = 0$. The angle i is equal to

$$i = \cos^{-1}(I_1/I_2), \quad 0 \le i \le \pi . \tag{B12}$$

2. Cartesian to action-angle

If the Cartesian position and momentum are known, then the procedure below gives action-angle variables.

(1) Evaluate L_x, L_y, and L_z using standard formulas. Then

$$I_1 = L_z ,$$
$$I_2 = (L_x^2 + L_y^2 + L_z^2)^{1/2} , \tag{B13}$$
$$\phi_1 = \tan^{-1}(L_y/L_x) + \frac{\pi}{2} .$$

The arctangent is defined to be positive for L_y positive and negative for L_y negative, so ϕ_1 has the sign of L_x.

(2) Calculate H_K and I_3 using

$$H_K = \frac{1}{2\mu}(p_x^2 + p_y^2 + p_z^2) - k/(x^2 + y^2 + z^2)^{1/2} ,$$

$$I_3 = (\mu k^2/-2H_k)^{1/2} .$$

Now I_1, I_2, I_3, and ϕ_1 are available.

(3) Evaluate the sign of the radial momentum,

$$\text{sgn} p_r = \text{sgn}(p_x \sin\theta_e \cos\phi_e + p_y \sin\theta_e \sin\phi_e + p_z \cos\theta_e) ,$$

where θ_e and ϕ_e are polar and azimuthal angles representing the position of the electron

$$\cos\theta_e = z/(x^2 + y^2 + z^2)^{1/2} ,$$

$$\tan\phi_e = (y/x) .$$

Always $0 \le \theta_e \le \pi$, and the sign of ϕ_e is the sign of y.

(4) Calculate the eccentricity e using Eq. (B1), and then calculate χ using the orbit equation (B4)

$$\chi = \pm\cos^{-1}\left[\left[\frac{I_2^2}{\mu k r} - 1\right] \Big/ e\right] .$$

The sign of χ must be taken to be the sign of p_r.

(5) Calculate ψ and ϕ_3 using Eqs. (B3) and (B2).

(6) Calculate the angle i between L and the z axis using

$$\cos i = L_z/(L_x^2 + L_y^2 + L_z^2)^{1/2} .$$

(7) Calculate the position of the particle in the plane of the orbit using two rotations

$$\begin{bmatrix} x'' \\ y'' \\ z'' \end{bmatrix} = A_2 A_1 \begin{bmatrix} x \\ y \\ z \end{bmatrix} ,$$

where the A's are defined in Eq. (B11). This must give $z'' = 0$.

(8) Evaluate $\chi + \phi_2$ using

$$\tan(\chi + \phi_2) = y''/x'' .$$

Then from χ and $\chi + \phi_2$, ϕ_2 is known.

---

*Present address: Joint Institute for Laboratory Astrophysics, University of Colorado, Boulder, CO 80309-0440.

[1] Recent reviews of the field of highly excited atoms in static fields include those of D. Kleppner, M. G. Littmann, and M. L. Zimmerman, in *Rydberg States of Atoms and Molecules*, edited by R. F. Stebbings and F. B. Dunning (Cambridge University, Cambridge, 1983), pp. 73—116; C. W. Clark, K. T. Lu, and A. F. Starace, in *Progress in Atomic Spectroscopy, Part C*, edited by H. J. Beyer and H. Kleinpoppen (Plenum, New York, 1984), pp. 247—320; R. H. Garstang, Rep. Prog. Phys. **40**, 105 (1977). Many other references are cited in Ref. 6(b).

[2] Reviews which concentrate on experimental work include those of J. C. Gay, in *Progress in Atomic Spectroscopy, Part C*, edited by H. J. Beyer and H. Kleinpoppen (Plenum, New York, 1984), pp. 177—246; H. Rottke, H. Zacharias, and K. H. Welge, in *Laser Techniques for Extreme Ultraviolet Spectroscopy*, AIP Conference Proceedings No. 90, edited by T. J. McIlrath and R. R. Freeman (AIP, New York, 1982), pp. 402—421; and P. M. Koch, in *Rydberg States of Atoms and Molecules*, edited by R. F. Stebbings and F. B. Dunning (Cambrige University, Cambridge, 1983), pp. 473—512.

[3] Quantum-mechanical calculations are very successful, if the principal quantum numbers n is not too large, but near the

ionization threshold, such calculations are much more difficult. A recent quantum calculation is that of D. Wintgen and H. Friedrich, Phys. Rev. Lett. **57**, 571 (1986). Semiclassical calculations include those of A. R. Edmonds, J. Phys. (Paris) Colloq. **31**, C4-71 (1970); A. F. Starace, J. Phys. B **6**, 585 (1973); A. R. P. Rau, Phys. Rev. A **16**, 613 (1977); J. A. C. Gallas, F. Gerck, and R. F. O'Connell, Phys. Rev. Lett. **50**, 324 (1983); W. P. Reinhardt, J. Phys. B **16**, L635 (1983); M. L. Du and J. B. Delos, Phys. Rev. Lett. **58**, 1731 (1987).

[4]C. W. Clark and K. T. Taylor, J. Phys. B **13**, L737 (1980); **15**, 1175 (1982); C. W. Clark, Phys. Rev. A **24**, 605 (1981).

[5]Note that the nucleus is taken to be infinitely massive. The finite nuclear mass corrections for a hydrogen atom in a uniform magnetic field were derived to first order in the electron-proton mass ratio by Lamb [W. Lamb, Phys. Rev. **85**, 259 (1952)]. O'Connell showed that these corrections are insignificant for states near the continuum [R. F. O'Connell, Phys. Lett. **70A**, 389 (1979)].

[6](a) J. B. Delos, S. K. Knudson, and D. W. Noid, Phys. Rev. Lett. **50**, 579 (1983); (b) Phys. Rev. A **28**, 7 (1983); (c) **30**, 1208 (1984); (d) D.W. Noid, S. K. Knudson, and J. B. Delos, Chem. Phys. Lett. **100**, 367 (1983).

[7](a) A. Messiah, *Quantum Mechanics* (Interscience, New York, 1961), Vol. I; (b) E. U. Condon and G. H. Shortley, *The Theory of Atomic Spectra* (Cambridge University Press, Cambridge, 1979), especially Chap. XVII, pp. 397—417, and Chap. III, pp. 48—53.

[8](a) D. Richards, J. Phys. B **16**, 749 (1983); (b) M. Robnik, J. Phys. A **14**, 3195 (1981).

[9](a) P. A. Braun and E. A. Solov'ev, J. Phys. B **17**, L211 (1984); (b) D. R. Herrick, Phys. Rev. A **26**, 323 (1982).

[10]Max Born, *The Mechanics of the Atom* (Unger, New York, 1960), Sec. 35, pp. 212—234.

[11]Geometrically, if the derivative of $h(I_2,\phi_2)$ in two distinct directions vanishes at a point, then that point must be a fixed point. $\partial h/\partial \phi_2$ vanishes at $I_2=I_1$ and at $I_2=I_3$. If a line of constant h transversely intersects either of these lines, then the point of intersection must be a fixed point. However, for all finite values of v/λ, the separatrices in question do not intersect the lines transversely, but join them smoothly, such that $(\partial I_2/\partial \phi_2)_h = 0$. This is visible at the top of the diagrams, not visible but true nevertheless at the bottom.

[12]A. Einstein, Verh. Dtsch. Phys. Ges. **19**, 82 (1917); L. Brillouin, J. Phys. (Paris) **7**, 353 (1926); J. B. Keller, Ann. Phys. (N.Y.) **4**, 180 (1958); V. P. Maslov, *Theorie des Perturbations et Methodes Asymptotiques* (Dunod, Paris, 1972); V. P. Maslov and M. V. Fedoriuk, *Semiclassical Approximation in Quantum Mechanics* (Reidel, Boston, 1981); R. A. Marcus, Faraday Discuss. Chem. Soc. **55**, 34 (1973).

[13]J. B. Delos, Adv. Chem. Phys. **65**, 161 (1986); S. K. Knudson, J. B. Delos, and B. Bloom, J. Chem. Phys. **83**, 5703 (1985); S. K. Knudson, J. B. Delos, and D. W. Noid, *ibid.* **84**, 6886 (1986).

[14]T. Poston and I. Stewart, *Catastrophe Theory and Its Applications* (Pitman, San Francisco, 1978); M. V. Berry, Adv. Phys. **25**, 1 (1976); J. N. L. Connor, Mol. Phys. **31**, 33 (1976); J. B. Delos, J. Chem. Phys. **86**, 425 (1986).

[15]P. A. Braun and E. A. Solov'ev, Zh. Eksp. Teor. Fiz. **86**, 68 (1984) [Sov. Phys.—JETP **59**, 492 (1984)]; E. A. Solov'ev, Zh. Eksp. Teor. Fiz. **34**, 278 (1981) [Sov. Phys.—JETP **34**, 265 (1981)]; Zh. Eksp. Teor. Fiz. **82**, 1762 (1982) [Sov. Phys.—JETP **55**, 1017 (1982)]; P. A. Braun, Zh. Eksp. Teor. Fiz. **84**, 850 (1983) [Sov. Phys.—JETP **57**, 492 (1983)].

[16]P. Cacciani, E. Luc-Koenig, J. Pinard, C. Thomas, and S. Liberman, Phys. Rev. Lett. **56**, 1467 (1986).